Publ. Astron. Soc. Japan (2015) 67 (1), 9 (1–12)
doi: 10.1093/pasj/psu135
Advance Access Publication Date: 2015 February 1

Suzaku studies of the supernova remnant CTB 109 hosting the magnetar 1E 2259+586

Toshio Nakano,[1,*] Hiroaki Murakami,[1] Kazuo Makishima,[1,2,3] Junoko S. Hiraga,[3] Hideki Uchiyama,[4] Hidehiro Kaneda,[5] and Teruaki Enoto[6,7]

[1]Department of Physics, Graduate School of Science, The University of Tokyo, 7-3-1 Hongo, Bunkyo-ku, Tokyo 113-0033, Japan
[2]MAXI Team, Institute of Physical and Chemical Research (RIKEN), 2-1 Hirosawa, Wako-shi, Saitama 351-0198, Japan
[3]Research Center for the Early Universe, The University of Tokyo, 7-3-1 Hongo, Bunkyo-ku, Tokyo 113-0033, Japan
[4]Science Education, Faculty of Education, Shizuoka University, 836 Ohya, Suruga-ku, Shizuoka 422-8529, Japan
[5]Goddard Space Flight Center, NASA, Greenbelt, MD 20771, USA
[6]Graduate School of Science, Nagoya University, Chikusa-ku, Nagoya, Aichi 464-8602, Japan
[7]RIKEN Nishina Center, 2-1 Hirosawa, Wako-shi, Saitama 351-0198, Japan

*E-mail: nakano@juno.phys.s.u-tokyo.ac.jp

Received 2014 February 12; Accepted 2014 October 24

Abstract

Ages of the magnetar 1E 2259+586 and the associated supernova remnant CTB 109 were studied. Analyzing the Suzaku data of CTB 109, its age was estimated to be ~ 14 kyr, which is much younger than the measured characteristic age of 1E 2259+586, 230 kyr. This reconfirms the previously reported age discrepancy of this magnetar/remnant association, and suggests that the characteristic ages of magnetars are generally over-estimated as compared to their true ages. This discrepancy is thought to arise because the former are calculated without considering decay of the magnetic fields. This novel view is supported independently by much stronger Galactic-plane concentration of magnetars than other pulsars. The process of magnetic field decay in magnetars is mathematically modeled. It is implied that magnetars are much younger objects than previously considered, and can dominate new-born neutron stars.

Key words: ISM: supernova remnants — stars: magnetars — stars: magnetic fields — stars: neutron — X-rays: individual (CTB 109, 1E 2259+586)

1 Introduction

1.1 Relations between magnetars and SNRs

27 Galactic and Magellanic X-ray sources are thought to constitute a class of objects called magnetars, which are single neutron stars (NSs) with extremely strong magnetic fields of $B = 10^{14–15}$ G. They are believed to shine (mainly in X-ray) by consuming the energies in their strong magnetic fields, because their X-ray luminosities exceed their spin-down luminosities and they are not likely to be accreting objects. The magnetar concept explains other peculiar

characteristics of these objects well, such as long pulse periods clustered in a narrow range (2–11 s), relatively large period derivatives, and unpredictable sporadic burst activities. However, we do not know yet how they are formed and how such strong fields evolved.

Supernova remnants (SNRs) associated with magnetars are expected to provide us with valuable clues to the scenario of magnetar production (e.g., Vink 2008; Safi-Harb & Kumar 2013). As a result, the study of SNR/NS associations (e.g., Seward 1985; Chevalier 2005, 2011) has been re-activated since the concept of magnetars has emerged. Although no clear difference in the explosion energy has yet been found between SNRs with and without magnetars (e.g., Vink & Kuiper 2006), an X-ray metallicity study of the SNR Kes 73, hosting the magnetar 1E 1841−045, led Kumar et al. (2014) to infer that the progenitor of this system had a mass of $\gtrsim 20\ M_{\odot}$, where $M_{\odot}$ is the solar mass. Through investigations of several SNR/magnetar associations, Safi-Harb and Kumar (2013) characterized environments that are responsible for the magnetar production, and reinforced the view of rather massive progenitors.

Apart from the progenitor issue, one particularly interesting aspect of magnetars, which can be studied by simultaneously considering the associated SNRs, is their age comparison. Of course, as discussed by Gaensler (2004), the ages of a magnetar and of the associated SNR, estimated independently, must agree for them to be regarded as a true association. However, these two age estimations sometimes disagree even in pairs with very good positional coincidence, including the 1E 2259+586/CTB 109 pair which is the topic of the present paper. This is often called the "age problem." While Allen and Horvath (2004) suspected that the problem arises because an SNR age estimate is affected by the presence of a magnetar, Colpi, Geppert, and Page (2000) instead attributed it to the magnetic field decay of magnetars, which can make their characteristic ages much longer than their true ages. After the discovery of SGR 0418+5729 (Rea et al. 2010), a magnetar with a low dipole magnetic field, the field's decay scenario has become more attractive (Dall'Osso et al. 2012; Igoshev 2012).

Through X-ray studies of CTB 109, the present paper attempts to address two issues. One is to solve the age problem with the 1E 2259+586/CTB 109 system, and the other is conversely to utilize the result to reinforce the nature of magnetars as magnetically driven NSs. After a brief introduction to the target system (section 2), we describe in section 3 and section 4 recent Suzaku observations of CTB 109, and reconfirm the age problem in the system (section 5). Then, an attempt is made in section 6 to solve it by invoking the decay of magnetic fields. Finally, we discuss some implications for the general view of NSs, including in particular their magnetic evolution. Other topics will be discussed elsewhere, including more detailed X-ray diagnostics of CTB 109, the origin of its peculiar half-moon shape, and characterization of the progenitor.

2 Magnetar 1E 2259+586 and SNR CTB 109

2.1 CTB 109

The Galactic SNR, CTB 109, hosting the central point X-ray source 1E 2259+586, was first discovered by the Einstein Observatory (Gregory & Fahlman 1980) as an extended X-ray source with a peculiar semi-circular shape. It was independently identified as a shell-type SNR by radio observations at 610 MHz (Hughes et al. 1981). A 10-GHz radio map taken with the Nobeyama Radio Observatory revealed good positional coincidence between the radio and X-ray shells, while it also detected no significant enhancement from 1E 2259+586 (Sofue et al. 1983).

Through CO molecular line observations, Heydari-Malayeri, Kahane, and Lucas (1981) and Tatematsu et al. (1985, 1987) found a giant molecular cloud located next to CTB 109, and suggested that it may have disturbed the SNR on the west side. Sasaki et al. (2004) conducted a comprehensive X-ray study of this SNR with XMM-Newton. Assuming a distance of $D = 3.0$ kpc (Kothes et al. 2002; Kothes & Foster 2012), they estimated the shock velocity, age, and the explosion energy as $\upsilon_{\rm s} = 720 \pm 60$ km s^{-1}, 8.8 kyr, and $(7.4 \pm 2.9) \times 10^{50}$ erg, respectively. Strong evidence for an interaction between the SNR shock front and the CO cloud was found by using ^{12}CO, ^{13}CO and Chandra observations (Sasaki et al. 2006). Furthermore, gamma-ray emission was detected with the Fermi-Lat from CTB 109 (Castro et al. 2012). Finally, using Chandra, Sasaki et al. (2013) detected emission from the ejecta component and refined the age to 14 kyr.

2.2 1E 2259+586

The compact object 1E 2259+586 was first detected in X-rays nearly at the center of CTB 109 (Gregory & Fahlman 1980). It was soon found to be a pulsar, and the pulse period was at first considered as $P = 3.49$ s (Fahlman et al. 1982). This was due to the double-peaked pulse profile, and the fundamental period was soon revised to $P = 6.98$ s (Fahlman & Gregory 1983). Repeated X-ray observations enabled the spin-down rate to be measured as $\dot{P} = (3\text{–}6) \times 10^{-13}$ s s^{-1} (Koyama et al. 1987; Hanson et al. 1988; Iwasawa et al. 1992), and these results made it clear that the spin-down luminosity of 1E 2259+586 (5.6×10^{31} erg s^{-1}) is far too insufficient to explain its X-ray luminosity, 1.7×10^{34} erg s^{-1}. Due to this and the long pulse period, 1E 2259+586 was long thought to be an

Table 1. Log of Suzaku observations of CTB 109.

Observation ID	α	δ	Start time	Exposure (ks)
404076010	$23^{h}01^{m}04\overset{s}{.}08$	$58^{\circ}58'15\overset{''}{.}6$	2009-05-25 20:00:17	122.6
506037010	$23^{h}01^{m}06\overset{s}{.}96$	$59^{\circ}00'50\overset{''}{.}4$	2011-12-13 06:48:41	40.8
506038010	$23^{h}00^{m}26\overset{s}{.}88$	$58^{\circ}44'13\overset{''}{.}2$	2011-12-14 04:47:02	41.4
506039010	$23^{h}03^{m}06\overset{s}{.}96$	$58^{\circ}58'51\overset{''}{.}6$	2011-12-15 01:57:25	30.4
506040010	$23^{h}03^{m}06\overset{s}{.}96$	$58^{\circ}40'51\overset{''}{.}6$	2011-12-15 18:03:52	30.5

X-ray binary with an orbital period of $\sim$2300 s (e.g., Fahlman et al. 1982), and extensive searching for a counterpart continued (Davies et al. 1989; Coe & Jones 1992; Coe et al. 1994). However, no counterpart was found (Hulleman et al. 2000), and instead, tight upper limits on the orbital Doppler-modulation have been obtained as $a_x \sin i < 0.8$ Lt-s (Koyama et al. 1989), $a_x \sin i < 0.6$ Lt-s (Mereghetti et al. 1998), and $a_x \sin i < 0.028$ Lt-s (Baykal et al. 1998). Here, a_x is the semi-major axis of the pulsar's orbit, and i is the orbital inclination. These strange properties of 1E 2259+586 led this and a few other similar objects to be called Anomalous X-ray Pulsars (AXPs).

In the 1990s, several attempts were made to explain 1E 2259+586 without invoking a companion: e.g., the massive white dwarf model (Usov 1994), and the precessing white dwarf model (Pandey 1996). Monthly observations of 1E 2259+596 over 2.6 yr with RXTE gave phase-coherent timing solutions indicating a strong stability over that period (Kaspi et al. 1999). This favored a non-accretion interpretation. Heyl and Hernquist (1999) suggested that spin-down irregularities of AXPs are statistically similar to glitches of radio pulsars. Meanwhile, the concept of magnetars was proposed to explain Soft Gamma Repeaters (SGRs) as magnetically powered NSs, namely, magnetars (Duncan & Thompson 1992; Thompson & Duncan 1995). Furthermore, like SGRs, 1E 2259+586 showed an X-ray outburst (Kaspi et al. 2002; Gavriil et al. 2004; Woods et al. 2004). Today, AXPs, including 1E 2259+586, and SGRs are both considered to be magnetars. Employing the canonical assumption of spin-down due to magnetic dipole radiation, the measured pulse period of $P = 6.98$ s (Iwasawa et al. 1992), and its derivative, $\dot{P} = 4.8 \times 10^{-13}$ s s^{-1} (e.g., Gavriil & Kaspi 2002), give a dipole magnetic field of 5.9×10^{13} G and a characteristic age of $\tau_c = P/2\dot{P} = 230$ kyr.

3 Observations and data reduction

The Suzaku observations of 1E 2259+586 and CTB 109 were made on two occasions. The first of them was conducted on 2009 May 25 as a part of the AO4 Key Project on magnetars (Enoto et al. 2010). The three cameras (XIS0, XIS1, and XIS3) of the X-ray Imaging Spectrometer (XIS) onboard Suzaku were operated in 1/4-window mode with a time resolution of 2 s (Koyama et al. 2007), to study the 6.98-s pulsation. The rectangular ($17' \times 4\overset{'}{.}3$) fields of view of the 1/4-window were centered on this magnetar, while the SNR was partially covered. For the second observation we performed four new pointings on to CTB 109 with Suzaku (PI: T. Nakano) on 2011 December 13. In order to synthesize a whole image of the SNR, all XIS cameras were operated in full-window mode under the sacrifice of time resolution. A log of these observations is given in table 1.

In the present work, we use the XIS data which were prepared with version 2.7.16.31 pipeline proceeding, and the calibration data that were updated in 2013 January. The data of the Hard X-ray Detector (HXD) from both observations are not utilized here, since the Suzaku data analysis in the present paper focuses on CTB 109, rather than the central magnetar. The data reduction was carried out using the HEADAS software package version 6.13, and spectral fitting was performed with `xspec` version 12.8.0. The redistribution matrix files and the auxiliary response files of the XIS were generated with `xisrmfgen` and `xissimarfgen` (Ishisaki et al. 2007), respectively.

4 Data analysis and result

4.1 Image analysis

Figure 1 shows a gray-scale mosaic image of CTB 109 obtained with the Suzaku XIS, shown after subtracting non X-ray background. The magnetar, 1E 2259+586, appears as a bright source at the center. The criss-cross region including 1E 2259+586 was taken in the first observation, while four square regions represent those from the second one. Thus, the mosaic XIS image reconfirms the half-moon-like morphology of this SNR (subsection 2.1).

As mentioned in subsection 2.1, the lack of a western part of CTB 109 is usually attributed to its interactions with giant molecular clouds. Bright regions in the SNR are also thought to be the signature of such an interaction (Sasaki et al. 2006). These issues, together with detailed spatial distributions of X-ray spectral properties, will be postponed to another publication. The present paper instead deals with average X-ray spectra, because our prime motivation is to estimate the age of CTB 109.

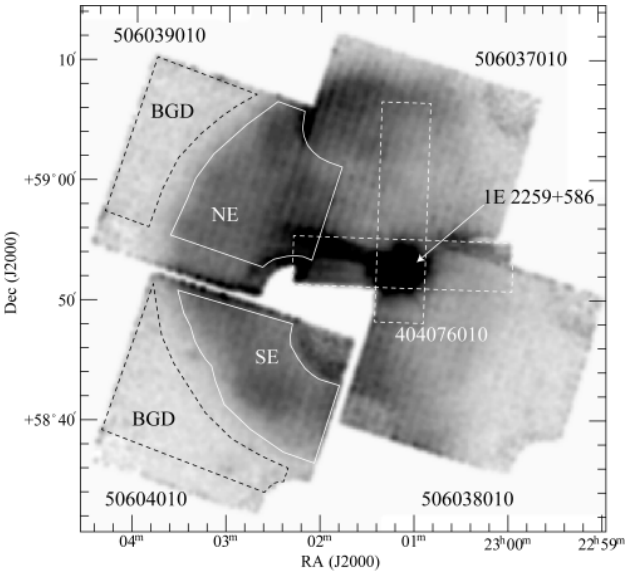

Fig. 1. A mosaic image of CTB 109 obtained in 0.4–5.0 keV with the Suzaku XIS. After subtracting the non X-ray background, the image was corrected for exposure and vignetting. The on-source and background regions are indicated by white and dashed black lines, respectively. Some corners of the square XIS fields of view are masked to remove calibration isotopes.

4.2 Spectral analysis

Figure 2 shows XIS0, XIS1, and XIS3 spectra of CTB 109 from the second observation, extracted from the regions indicated in figure 1 as "NE" and "SE", which represent two eastern pointing positions. Since these eastern parts of the SNR have kept a smooth round shape, the effect from the interaction with GMC (giant molecular cloud) seems to be small. Background spectra were extracted from source-free regions in the same observation and are indicated as "BGD" in figure 1. Spectral bins were summed up to attain a minimum of 30 counts bin^{-1}. The "NE" and "SE" spectra are very similar and both exhibit emission lines due to highly ionized atoms such as a Ne IX triplet ($\sim$0.92 keV), a Ne X Lyα (1.02 keV), a Mg XI triplet ($\sim$1.35 keV), a Si XIII triplet ($\sim$1.87 keV), and a S XV triplet ($\sim$2.45 keV).

We first applied a variable-abundance non-equilibrium ionization (VNEI) plasma emission model to the NE spectra in figure 2a. However, even when abundances of Ne, Mg, Si, and S are allowed to vary freely, the reduced χ^2 of the fit was not made lower than 1.5. Thus, the single-temperature VNEI model was rejected. Other plasma models in `xspec`, such as `vpshock` and `vmekal`, were also unsuccessful.

Then, we considered that the SNR emission consists of two components including ejecta and shocked interstellar media (ISM), and added a non-equilibrium ionization (NEI) plasma emission model to model shocked ISM component. The abundance of the ISM components was fixed to solar to reduce the number of free parameters.

By introducing this two-component emission model, the fit was improved to $\chi^2/\nu = 1.28$. Since different XIS cameras gave discrepant fit residuals around Mg XI Kα and Si XIII Kα lines, presumably due to calibration uncertainties of the XIS, we allowed gain parameters of the XIS cameras to vary. Then, the fit became acceptable with $\chi^2/\nu = 1.06$ (1293/1223). The obtained best-fitting parameters are shown in table 2, while the gain parameters are shown in table 3. Since the obtained abundances of the second (Plasma 2) component are all consistent with 1 solar, it is also likely to be dominated by the ISM. The two components are both inferred to be somewhat deviated from ionization equilibrium. The fit was not improved even when the abundance of the Plasma 2 component is allowed to change from 1.0. Similarly, we analyzed the SE spectra shown in figure 2b, and derived the parameters which are again summarized in table 2. Thus, the two temperatures are in good agreement between the two regions, although the SE region gives somewhat higher metal abundances. This

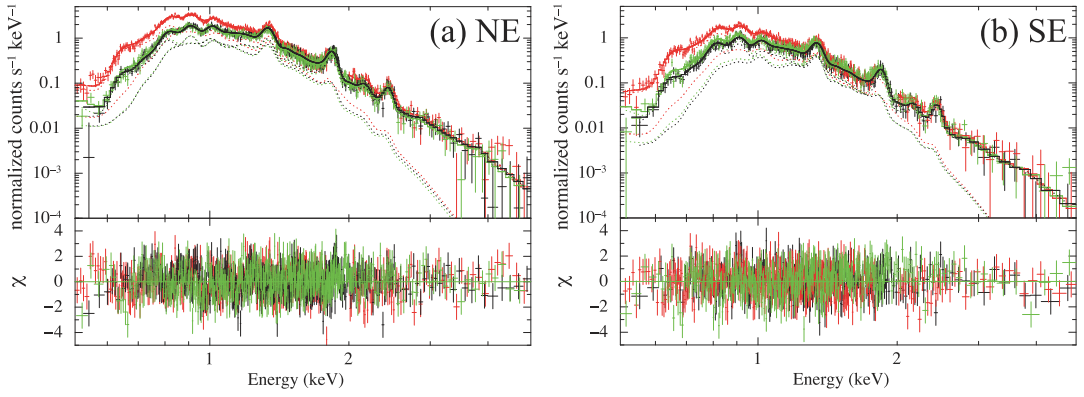

Fig. 2. Background-subtracted XIS0 (black), XIS1 (red), and XIS3 (green) spectra of CTB 109, extracted from the NE (panel a) and SE (panel b) regions. They are fitted simultaneously with a two-component model described in the text. The dotted lines indicate individual model components, with the three colors specifying the three cameras. (Color online)

Table 2. Best-fit spectrum parameters for the NE and SE regions.*

Component	Parameter	NE	SE
Absorption	$N_{\rm H}(10^{22}{\rm cm}^{-2})$	0.78 ± 0.01	$0.73^{+0.01}_{-0.02}$
Plasma 1 (VNEI)	kT_1	$0.62^{+0.04}_{-0.01}$	$0.65^{+0.02}_{-0.01}$
	$\eta_1{}^{\dagger}$ $(10^{12}{\rm cm}^{-3}{\rm s})$	$0.37^{+0.05}_{-0.04}$	$0.22^{+0.05}_{-0.06}$
	Ne (solar)	0.8 ± 0.2	$0.8^{+0.2}_{-0.1}$
	Mg (solar)	$0.88^{+0.01}_{-0.06}$	1.1 ± 0.1
	Si (solar)	1.2 ± 0.1	$1.7^{+0.1}_{-0.3}$
	S (solar)	1.0 ± 0.1	$1.7^{+0.2}_{-0.3}$
	Fe (solar)	$0.99^{+0.05}_{-0.06}$	$1.0^{+0.2}_{-0.1}$
	$K_1{}^{\ddagger}$ $(10^{-2}{\rm cm}^{-5})$	$3.7^{+0.2}_{-0.1}$	1.2 ± 0.1
Plasma 2 (NEI)	kT_2	0.26 ± 0.01	0.25 ± 0.01
	$\eta_2{}^{\dagger}$ $(10^{12}{\rm cm}^{-3}{\rm s})$	> 1	> 1
	Abundance (solar)	1 (fixed)	1 (fixed)
	$K_2{}^{\ddagger}$ $(10^{-2}{\rm cm}^{-5})$	$19.6^{+0.8}_{-1.4}$	$13.2^{+0.8}_{-1.6}$
χ^2/dof		1294/1223	1138/951

*Uncertainties are statistical errors at 90% confidence.
†Ionization parameter, defined as $\eta = n_{\rm e}t$.
‡Normalization of NEI or VNEI, defined as $K = \frac{10^{-14}}{4\pi D^2}\int n_{\rm e} n_{\rm H} dV$.

Table 3. The best-fitting gain parameters.*

Region	Instrument	Slope	Offset (eV)
NE	XIS0	0.997 ± 0.001	-5.3 ± 0.2
	XIS1	1.004 ± 0.001	-3.0 ± 0.3
	XIS2	0.986 ± 0.001	-7.0 ± 0.4
SE	XIS0	1.003 ± 0.001	-10.6 ± 0.1
	XIS1	0.993 ± 0.001	6.6 ± 0.1
	XIS2	0.985 ± 0.001	6.6 ± 0.2

*Uncertainties are statistical errors at 90% confidence.

two-component emission model was also employed by Sasaki et al. (2013).

5 Estimation of the age of CTB 109

Now that the average plasma properties of CTB 109 have been quantified, let us proceed to our prime goal of studying this SNR, i.e., its age estimation. First, the physical radius of CTB 109 is estimated as $R = (16 \pm 1)d_{3.2}$ pc , from its angular size of $\sim 16'$ and the estimated distance $D = 3.2 \pm 0.2$ kpc (Kothes & Foster 2012). Here, $d_{3.2} = D/3.2$ is the scale factor of distance. Next, CTB 109 may be considered in the Sedov phase (neglecting the missing western part). Then, applying the Sedov–Taylor similarity solution (Sedov 1959; Taylor 1950) to this SNR, its age can be obtained as

$$\tau_{\rm SNR} = \frac{2}{5}\frac{R}{v_{\rm s}} \tag{1}$$

where $v_{\rm s}$ again represents the shock front velocity.

Assuming the strong shock limit, we can calculate $v_{\rm s}$ from the post-shock temperature $T_{\rm ps}$ as

$$v_{\rm s} = \sqrt{\frac{16}{3\bar{m}}kT_{\rm ps}} \tag{2}$$

where k and $\bar{m}$, respectively, represent the Boltzmann constant and the mean mass per free particle. Assuming a solar abundance (subsection 4.2), we employed $\bar{m} \simeq 0.61 m_{\rm p}$ where $m_{\rm p}$ is the proton mass. Since CTB 109 is a middle-aged SNR without too strong shocks, the electron temperature of the NEI component measured in section 4 can be considered to be close to the kinematic ISM temperature, and hence to $T_{\rm ps}$ (Ghavamian et al. 2007). Thus, substituting 0.25 ± 0.02 keV for $T_{\rm ps}$, equation (2) gives $v_{\rm s} = 460 \pm 40$ km s^{-1}, and then equation (1) yields $\tau_{\rm SNR} \simeq (14 \pm 2)d_{3.2}$ kyr in agreement with Sasaki et al. (2013). Compared to the estimated $\tau_{\rm SNR}$, the characteristic age of 1E 2259+586, $\tau_{\rm c} = 230$ kyr (subsection 2.2), is ~ 16 times larger.

If we assume that CTB 109 is in a cooling phase rather than the Sedov phase, the time dependence of the radius becomes $R \propto t^{2/7}$ (McKee & Ostriker 1977). Then, the age estimation slightly changes, to

$$\tau_{\rm SNR} = \frac{2}{7}\frac{R}{v_{\rm s}}, \tag{3}$$

and $\tau_{\rm SNR} = (10 \pm 1)d_{3.2}$ kyr is obtained. Therefore the age discrepancy still persists (even increases).

Let us cross-check the above estimates using the parameter $\eta \equiv n_{\rm e}t$ (table 2) of the ejecta component. We assume that the SNR has a half spherical shell with thickness of $\Delta R = R/12$ (assuming $4/3\pi R^3 n_0 m_{\rm p} = 4\pi R^2 \Delta R n_0 m_{\rm p}$), and the ISM component corresponding to Plasma 2 in table 2 is emitted from this shell. Furthermore, as a simplest approximation, the ejecta component (Plasma 1 in table 2) may be assumed to uniformly fill the inner region, considering that the reverse shock has reached the center of the SNR. In the NE region, the extracted emission volumes of Plasma 1 (ejecta) and Plasma 2 (ISM) can be obtained numerically as $V_1 = 4.0 \times 10^{58} d_{3.2}^3$ cm^3 and $V_2 = 1.4 \times 10^{58} d_{3.2}^3$ cm^3, respectively. Then, the spectrum normalizations in table 2 give the averaged density of the ejecta as $n_1 = (0.33 \pm 0.03)d_{3.2}^{-1/2}$ cm^{-3} and that of the ISM shell as $n_2 = (1.2 \pm 0.1)d_{3.2}^{-1/2}$ cm^{-3}. The time required for the ejecta to become ionized as we now observe is hence estimated as $\eta/n_1 = (29 - 34)d_{3.2}^{1/2}$ kyr. Applying the same argument to the SE region having the emission volumes of $V_1 = 6.7 \times 10^{57} d_{3.2}^3$ cm^3 and $V_2 = 3.3 \times 10^{57} d_{3.2}^3$ cm^3, we obtain $n_1 = (0.46 \pm 0.05)d_{3.2}^{-1/2}$ cm^{-3} and $n_2 = (0.55 \pm 0.06)d_{3.2}^{-1/2}$ cm^{-3}, and $\eta/n_1 = (11 - 19)d_{3.2}^{1/2}$ kyr. Pre-shock density is estimated as $n_0 = n_2/4 = (0.1 - 0.3)d_{3.2}^{-1/2}$ cm^{-3}.

Even though these estimates of $\tau_{\rm SNR}$ must have a certain range of systematic uncertainties, large discrepancies significantly remain between $\tau_{\rm SNR}$ and $\tau_{\rm c}$. In fact, it would be difficult to think that CTB 109 are emitting X-rays even at an age of 230 kyr while keeping the regular shape (except the missing western half), because its density environment as estimated is quite typical of a solar neighborhood. Thus, we reconfirm the previously reported age discrepancy (Sasaki et al. 2013) between CTB 109 and 1E 2259+586.

6 Solving the age discrepancy

The magnetar 1E 2259+586 is located nearly at the very center of the half-moon-shaped shell of CTB 109 (subsection 4.1, figure 1). This coincidence is difficult to explain by invoking a chance superposition of the two objects. We therefore assume that 1E 2259+586 and CTB 109 were indeed produced by the same supernova explosion (subsection 1.1), while $\tau_{\rm c}$ of 1E 2259+586 is somehow significantly overestimated, compared to its true age which we consider to be close to $\tau_{\rm SNR}$.

6.1 Case with a constant magnetic field

To solve the issue of the suggested overestimation of $\tau_{\rm c}$ after Colpi, Geppert, and Page (2000) and Dall'Osso, Granot, and Piran (2012), let us begin with reviewing the meaning of $\tau_{\rm c}$. In general, the spin evolution of a pulsar with dipole surface magnetic field B is expressed empirically as

$$\frac{d\omega}{dt} = -bB^2\omega^n \tag{4}$$

with $b \equiv 32\pi^3 R_{\rm psr}^6/3I\mu_0 c^3$ and a braking index of $n = 3$, where $R_{\rm psr} = 10$ km is the pulsar's radius, $I = 9.5 \times 10^{44}$g cm^2 its momentum of inertia, μ_0 the vacuum permeability and c the light velocity. If we use the pulse period $P = 2\pi/\omega$ and its derivative $\dot{P}$ instead of ω and $\dot{\omega}$, equation (4) becomes

$$B = \sqrt{\frac{P\dot{P}}{b}} \simeq 3.2 \times 10^{19}\sqrt{P\dot{P}}\ {\rm G}. \tag{5}$$

If B does not depend on time t, equation (4) can be integrated as

$$t = -\frac{1}{n-1}\left(\frac{\omega}{\dot{\omega}}\right)\left[1-\left(\frac{\omega}{\omega_0}\right)^{n-1}\right] = \tau_{\rm c}\left[1-\left(\frac{\omega}{\omega_0}\right)^{n-1}\right] \tag{6}$$

where ω and $\dot{\omega}$ both refer to the present values, while ω_0 is the angular frequency at $t = 0$ (i.e., the birth). Assuming that $(\omega/\omega_0)^{n-1}$ can be neglected, the characteristic age is defined as

$$\tau_{\rm c} \equiv \frac{\dot{\omega}}{(n-1)\,\omega} \equiv \frac{P}{(n-1)\,\dot{P}}. \tag{7}$$

These equations are generally used for pulsars and are found in some textbooks (e.g., Lyne & Graham-Smith 1998).

More generally, the true age of the pulsar, denoted by t_0, can be compared with its $\tau_{\rm c}$ as

$$\frac{\tau_{\rm c}}{t_0} = \frac{1}{1-\left(\frac{\omega}{\omega_0}\right)^{n-1}} = \frac{1}{1-\left(\frac{P_0}{P}\right)^{n-1}} \simeq 1+\left(\frac{P_0}{P}\right)^{n-1}, \tag{8}$$

where $P_0 = 2\pi/\omega_0$, and the last expression is the first-order approximation in $(P_0/P)^{n-1}$. Thus, $\tau_{\rm c}$ becomes somewhat larger than t_0 if $(P_0/P)^{n-1}$ cannot be neglected. Conversely, if we somehow have an independent estimate of t_0 its comparison with $\tau_{\rm c}$ can be used to infer P_0 as

$$P_0 = P\left(-\frac{t_0}{\tau_{\rm c}}+1\right)^{1/(n-1)}. \tag{9}$$

For example, the Crab pulsar (Staelin & Reifenstein 1968), with $P = 33$ ms, $\dot{P} = 2.42 \times 10^{-13}$s s^{-1} and $n = 2.509$ (Lyne et al. 1993), has $\tau_{\rm c} = 1241$ yr. Comparing this with its true age of 960 yr (as of 2014), equation (9) yields $P_0 = 18$ ms if assuming $n = 2.509$, or $P_0 = 15.7$ ms if $n = 3.0$ (for ideal magnetic dipole radiation). Thus, regardless of the employed value of n, the small difference between $\tau_{\rm c}$ and t_0 of the Crab pulsar can be understood to imply that it has so far lost $\sim 3/4$ of its initial rotational energy in ~ 1 kyr.

In contrast to the above case of young active pulsars, we would need to invoke $P_0 = P \times 0.97 = 6.76$ s, if equation (9) with $n = 3$ were used to explain the large discrepancy, $\tau_{\rm c}/t_0 \sim \tau_{\rm c}/\tau_{\rm SNR} \sim 16$, found in the CTB/1E 2259+586 system. This would lead to a view that 1E 2259+586 was born some 14 kyr ago as a slow rotator of which the spin period is much longer than those (0.2 to 2 s) of the majority of *currently* observed (hence relatively old) radio pulsars, and has so far lost only a tiny fraction of its rotational energy in 14 kyr. However, such a view is opposite to a general consensus that new-born magnetars must be rotating rapidly, even faster than ordinary pulsars, in order for them to acquire their strong magnetic fields (e.g., Usov 1992; Duncan & Thompson 1996; Lyons et al. 2010). Furthermore, an NS with $P_0 = 6.67$ s has an angular momentum of only $\sim 10^{-5}$ of those of typical new-born pulsars with $P_0 \sim 10$ ms, including the Crab pulsar, and hence would require extreme fine tuning in the progenitor-to-NS angular momentum transfer during the explosion. We therefore conclude that the age problem of

1E 2259+586 cannot be solved as long as its magnetic field is assumed to have been constant since its birth.

6.2 Effects of magnetic field decay

Since the age problem of 1E 2259+586/CTB 109 cannot be solved as long as B is considered constant, we may next examine the case where B decays with time (subsection 1.1). In fact, the X-ray emission of magnetars is thought to arise when their magnetic energies are consumed (Thompson & Duncan 1995). Then, the calculations presented in subsection 5.1 would be no longer valid, and we need to integrate equation (6) considering the time evolution of B.

Let us consider a simple magnetic field decay model employed by Colpi, Geppert, and Page (2000), namely

$$\frac{dB}{dt} = -aB^{1+\alpha}, \tag{10}$$

where $\alpha \geq 0$ is a parameter, and a is another positive constant. This equation can be solved as

$$B(t) = \begin{cases} \dfrac{B_0}{\left(1+\dfrac{\alpha t}{\tau_{\rm d}}\right)^{1/\alpha}} & (\alpha \neq 0) \\ B_0 \exp\left(\dfrac{-t}{\tau_{\rm d}}\right) & (\alpha = 0) \end{cases} \tag{11}$$

where B_0 represents the initial value of B, and $\tau_{\rm d} = \left(1/aB_0^{\alpha}\right)$, an arbitrary constant, means a typical lead time until the power-law like decay of B begins.

Substituting equation (11) into equation (4), we can derive P as a function of t.

Then, as already given by Dall'Osso, Granot, and Piran (2012), $\tau_{\rm c}$ can be expressed as a function of t, P_0, α, and $\tau_{\rm d}$ as

$$\tau_{\rm c} = \begin{cases} \dfrac{\tau_{\rm d}}{2-\alpha}\left\{\left[1+(2-\alpha)\dfrac{\tau_0}{\tau_{\rm d}}\right]\left(1+\dfrac{\alpha t}{\tau_{\rm d}}\right)^{2/\alpha} - \left(1+\dfrac{\alpha t}{\tau_{\rm d}}\right)\right\} & (\alpha \neq 0, 2) \\ \dfrac{\tau_{\rm d}}{2}\left[\left(1+\dfrac{2\tau_0}{\tau_{\tau_{\rm d}}}\right)\exp\left(\dfrac{2t}{\tau_{\rm d}}\right) - 1\right] & (\alpha = 0) \\ \left(1+\dfrac{2t}{\tau_{\rm d}}\right)\left[\tau_0 + \dfrac{\tau_{\rm d}}{2}\ln\left(1+\dfrac{2t}{\tau_{\rm d}}\right)\right] & (\alpha = 2) \end{cases} \tag{12}$$

where $\tau_0 \equiv P_0/2\dot{P}_0$ is the initial value of $\tau_{\rm c}$. The first form of equation (12) reduces to equation (8) for $\alpha \to \infty$ or $\tau_{\rm d} \to \infty$, i.e., the case of a constant B.

6.3 Magnetic field evolution of 1E 2259+586

Our next task is to examine whether the observed values of P and $\dot{P}$ of 1E 2259+586 can be explained with the picture presented in subsection 6.2. Equation (12) involves four free parameters, namely α, B_0 , $\tau_{\rm d}$, and P_0, whereas we have only two observables, P and $\dot{P}$ at $t = t_0 \simeq 14$ kyr. In subsection 5.1, we showed that the effect of P_0 can be neglected, when the current P is long enough. Therefore, we chose to fix P_0 at 3 ms where strong dynamo works efficiently (e.g., Duncan & Thompson 1996). To visualize effects of P_0, another solution with $P_0 = 10$, 100 ms and $\alpha = 1.2$ is also shown in figure 3 [panels (b), (c), and (d)]. Thus, the effects of P_0 are limited to very early ($\ll 1$s) stages of the evolution, and its value does not affect our discussion as long as it is much shorter than ~ 6.7 s.

Then, if α is specified, we can find a pair (B_0, $\tau_{\rm d}$) that can simultaneously explain P and $\dot{P}$ at present. Figure 3 shows the behavior of such a family of solutions to equation (12). Below, we try to constrain the values of α (hence of B_0 and $\tau_{\rm d}$), assuming that α is relatively common among magnetars. This is because the broad-band X-ray spectra of magnetars are determined rather uniquely by $\tau_{\rm c}$ (Enoto et al. 2010), so that $\tau_{\rm c}$ is considered to be tightly related to t_0 even if these two are unlikely to be identical: object-to-object scatter in α would cause a scatter in the $\tau_{\rm c}/t_0$ ratio, and would make the relation of Enoto et al. (2010) difficult to interpret.

When α is small ($0 \leq \alpha < 0.5$), the field would decay, as seen in equation (10), either exponentially (if $\alpha = 0$) on a time scale of $\tau_{\rm d}$, or (if $\alpha \neq 0$) with a relatively steep power-law after a long lead time $\tau_{\rm d} \sim t_0$. The required initial field, $B_0 \sim 10^{15}$ G, is reasonable. However, the implied view would be rather ad-hoc: 1E 2259+586 had been relatively inactive until recently, when it suddenly started to release its magnetic energy at a high rate. Furthermore, if such a small value of α were common to magnetars, their age differences would make, as in figure 3a, their present-day field distribution scatter much more widely than is observed. Hence we regard these small values of α unlikely.

As α increases towards 2.0, the power-law field decay becomes milder, with shorter values of $\tau_{\rm d}$ and stronger initial fields B_0. The implication is that the object started releasing its magnetic energy rather soon after the birth, and had already dumped away a large fraction of its rotational energy at a very early stage when the field was still very strong. As seen in figure 3c, the spin period has almost converged to its terminal value (see also Dall'Osso et al. 2012). Therefore, this case can explain the observed narrow scatter in P of magnetars, assuming that they share relatively similar values of α and B_0. However, the cases with $\alpha \sim 2.0$ or larger

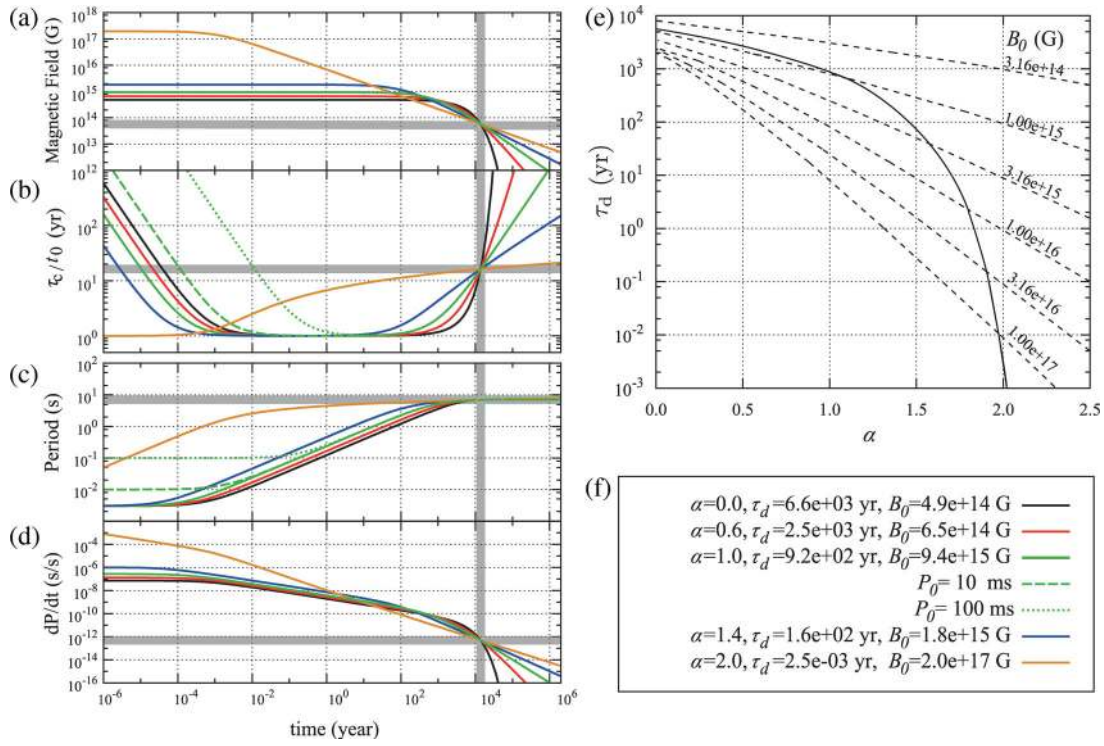

Fig. 3. Possible evolution tracks of 1E 2259+586 assuming equation (4) and equation (10). Panels (a)–(d) represent the behavior of the magnetic field B, the over-estimation factor of the characteristic age (i.e., τ_c/t_0), the pulse period P, and its time derivative $\dot{P}$, respectively. The six representative tracks are all constrained to reproduce the presently measured P and $\dot{P}$ at $t = 14$ kyr. The dashed and dotted ones assume $P_0 = 10$ ms and 100 ms, respectively, while the other five all $P_0 = 3$ ms. Panel (e) shows the trajectory of solutions that can explain the present-day ($t = 14$ kyr) 1E 2259+586. Dashed lines indicate the initial filed value B_0. Panel (f) summarize the parameter sets of the trajectories. (Color online)

would require too strong initial fields, e.g., $B_0 \sim 10^{17}$ G, which would be much higher than the strongest dipole field observed from magnetars, $B = 2.4 \times 10^{15}$ G of SGR 1806−20 (Nakagawa et al. 2009). Therefore, such large-α solutions are unlikely, too.

To summarize these examinations, figure 3e shows the locus of the allowed solutions on the (α, τ_d) plane, where the values of B_0 are also indicated. We thus reconfirm the above considerations, that the range of $1 \lesssim \alpha < 2$ is appropriate, in agreement with the suggestion by Dall'Osso, Granot, and Piran (2012). Some discussions follow in subsection 7.1.

7 Discussion

7.1 Comparison with other objects

We reconfirmed the age problem of 1E 2259+586 and CTB 109, and presented a way to solve it with a simple magnetic field decay model. The result agrees with the basic concept of magnetar hypothesis which implies that the energies stored by their magnetic fields should be consumed to supply their X-ray luminosities exceeding those available with their spin down. The amount of released

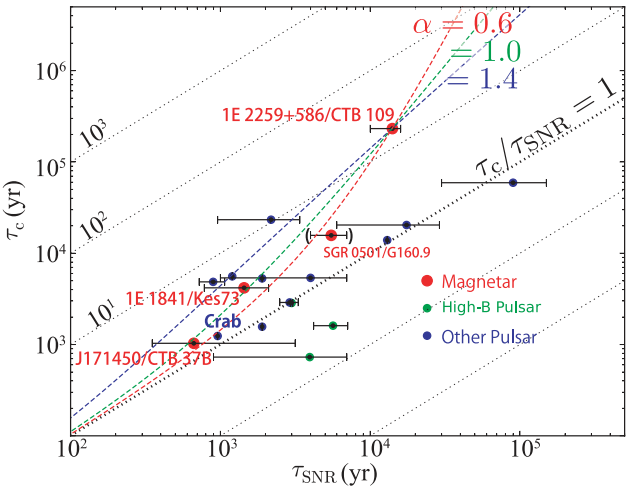

Fig. 4. Relations between τ_{SNR} and τ_c of single NSs associated with SNRs. Red, magenta and blue represent magnetars, high-B pulsars and rotation powered pulsars, respectively. Parameters are listed in table 4. The SGR 0501+4516/G160.9+2.6 pair is parenthesized, because the association is rather doubtful, and this SNR might be associated with another pulsar PSR B0458+46 (e.g., Leahy & Roger 1991). The red, green, and blue dashed curves indicate solutions to equation (12), with $(\alpha, \tau_d, B_0) = (0.6, 2.5 \times 10^3$ yr, 6.5×10^{14} G), (1.0, 9.2×10^2 yr, 9.4×10^{15} G) and (1.4, 1.6×10^2 yr, 1.8×10^{15} G), respectively. They all assume $P_0 = 3$ ms, and B_0 which is specified by figure 3e. (Color online)

field energies can be reflected in the overestimations of the characteristic ages.

Let us then examine whether this concept applies to other NS/SNR associations, including both magnetars and ordinary pulsars. Figure 4 shows relations between τ_c of such single pulsars and the ages of their host SNRs. Parameters of pulsar/SNR associations are listed in table 4. Data points of ordinary pulsars are distributed around the line representing $\tau_c/\tau_{SNR} = 1$ with a few exceptions (see e.g., Torii et al. 1999 for J1811−1925/G11.2−0.3). Therefore, radio pulsars, including the particular case of the Crab pulsar (subsection 6.1), are considered to be free from the age problem.

In addition to the ordinary pulsars, figure 4 shows a few other magnetar/SNR associations. The magnetar CXOU J171405.7−381031 has a very small characteristic age of 0.96 kyr (Sato et al. 2010), which is consistent, within rather large errors, with the age ($0.65^{+2.5}_{-0.3}$ kyr; Nakamura et al. 2009) of the associated SNR, CTB 37B. Another magnetar/SNR association, 1E 1841−045/Kes 73, is seen in figure 4 between J171405.7−381031/CTB 37B and 1E 2259+586/CTB 109. The age of Kes 73 was estimated by Kumar et al. (2014), as 0.75–2.1 kyr (table 4). Combining this with $\tau_c = 4.7$ kyr of 1E 1841−045 (table 4), the age discrepancy of this pair becomes $\tau_c/\tau_{SNR} = 2.7$–8. These two associations do not show large overestimation factors of τ_c/τ_{SNR} as much as the 1E 2259+586/CTB 109 association. Thus, the three magnetar/SNR associations (including 1E 2259+586/CTB 109) suggest that the age over-estimation factor, τ_c/τ_{SNR}, increases towards older objects. This agrees, at least qualitatively, with the theoretical behavior seen in figure 3c, as long as P_0 is negligible.

We hence tried to explain the data points of these three magnetar/SNR associations with a common set of parameters, and derive a plausible range of α.

For this purpose, three evolution tracks representing the solutions to equation (12) for 1E 12259+586/CTB 109 are additionally plotted on figure 4. Each parameter set is the same as that of figure 3f. If α is as small as $0 \leq \alpha < 0.6$ (dashed red line), the CXOU J171405.7−381031/CTB 37B association cannot be explained. On the other hand, a large value of $\alpha\,(> 1.5)$ fails to explain the 1E 1841−045/Kes 73 association. Thus, the three magnetar/SNR pairs in figure 4 can be explained in a unified way if they have a common value of α (and also of τ_d) that is in the range of $0.6 < \alpha < 1.4$.

7.2 Supporting evidence

The scenario so far developed implies that magnetars form a population that is much younger than previously thought. This important inference is supported by

Table 4. Parameters for figure 4.*,†

#	Pulsar/SNR	P (ms)	$\dot{P}$ (s s^{-1})	B ($\times 10^{12}$ G)	τ_c (kyr)	τ_{SNR} (kyr)
1	1E 1841−045/Kes 73	11778	4.5×10^{-11}	730	4	0.75–2.1
2	SGR 0501+4516/G160.9+2.6	5762	5.8×10^{-12}	190	16	4–7
3	J171405.7−381031/CTB 37B	3824	5.9×10^{-11}	480	0.96	$0.65^{+25}_{-0.3}$
4	1E 2259+586/CTB 109‡	6979	4.8×10^{-13}	58	230	10–16
5	J1846−0258/Kes 75	326	7.1×10^{-12}	49	0.7	0.9–4.3
6	J1119−6127/G292.2−0.5	407	4.0×10^{-12}	41	1.6	4.2–7.1
7	J1124−5916/G292.0+1.8	135	7.5×10^{-13}	10	2.9	2.93–3.05
8	J1513−5908/G320.4−1.2	151	1.5×10^{-12}	15	1.6	1.9
9	J0007+7303/G119.5+10.2	315	3.6×10^{-13}	11	14	13
10	J1930+1852/G54.1+0.3	136	7.5×10^{-13}	10	2.9	2.5–3.3
11	J1856+0113/W 44	267	2.1×10^{-13}	7.5	20	6–29
12	J0633+0632/G205.5+0.5	297	8.0×10^{-14}	4.9	60	30–150
13	Crab	33	4.2×10^{-13}	3.8	1.2	0.959
14	J0205+6449/3C 58	65	1.9×10^{-13}	3.6	5	1–7
15	J1833−1034/G21.5−0.9	61	2.0×10^{-13}	3.6	5	0.72–1.07
16	J1747−2809/G0.9+0.1	52	1.6×10^{-13}	2.9	5	1.9
17	J1813−1749/G12.8−0.0	44	1.3×10^{-13}	2.4	6	1.2
18	J1811−1925/G11.2−0.3	64	4.4×10^{-14}	1.7	2.3	0.96–3.4

*Data for P and $\dot{P}$ of pulsar were collected from ATNF Pulsar catalogue (Manchester et al. 2005). ⟨http://www.atnf.csiro.au/research/pulsar/psrcat⟩.

†Data for τ_{SNR} were collected from Ferrand and Safi-Harb (2012). ⟨http://www.physics.umanitoba.ca/snr/SNRcat⟩.

‡This work.

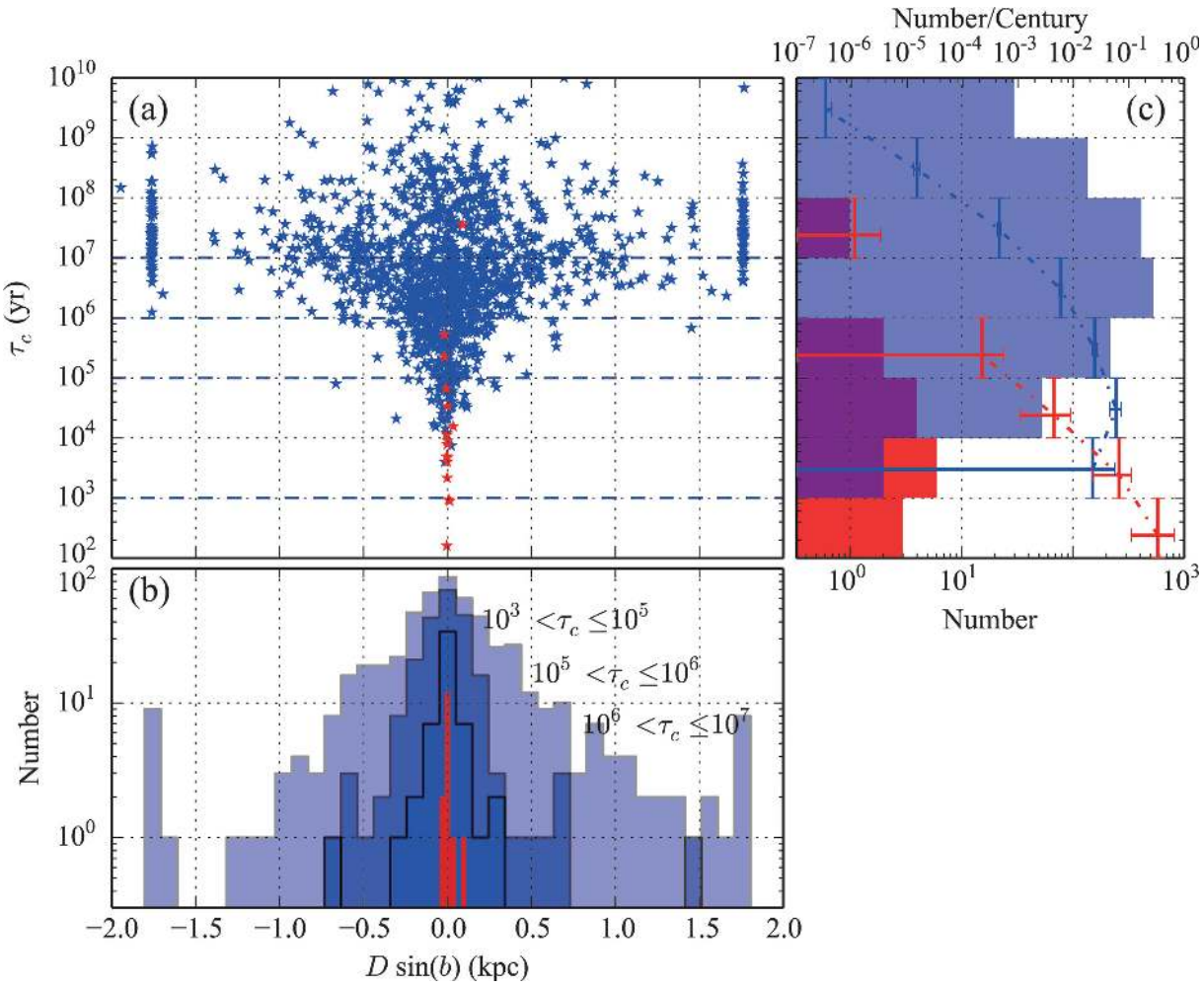

Fig. 5. (a) Spatial distributions of magnetars (red) and radio pulsars (blue). Abscissa and ordinate represent distance from the Galactic plane and characteristic age, respectively. (b) Projection of panel (a) on to the direction perpendicular to the Galactic plane. Radio pulsars are divided into three subgroups according to their age. (c) Age distributions of the objects, produced by projecting panel (a) on to the time axis. Histograms represent numbers of pulsars with ages in that logarithmic interval, while crosses tied by a dotted line show the object number per century. (Color online)

an independent piece of evidence. Figure 5 shows a spatial distribution of NSs including magnetars. Pulsars are kicked by explosions, and moving away from their birthplaces. Hence, older pulsars with larger τ_c are thus distributed to greater distances from the Galactic plane. In contrast, magnetars are much more concentrated to the plane for their nominal age, as better seen in figure 5b which is a projection of figure 5a along the direction perpendicular to the Galactic plane. This implies two possible scenarios; magnetars, as we have shown, are much younger than indicated by their τ_c, or their kick velocities are systematically lower than those of others. Recently, proper motions of four magnetars (SGR 1806−20, SGR 1900+14, 1E 2259+586, and 4U 0142+61) were successfully measured by Tendulkar, Cameron, and Kulkarni (2012, 2013). They calculated the mean and standard deviation of the ejection velocities as 200 km s^{-1} and 90 km s^{-1}, respectively. They also concluded that the weighted average velocity of magnetars is in good agreement with the tangential velocities of the pulsar population (Hobbs et al. 2005).

Therefore, we are left with the former of the two possibilities. In other words, magnetars should be systematically younger than ordinary pulsars that have similar τ_c.

7.3 Implication for the magnetar population

Observationally, magnetars are no longer a minority of NS species. This is shown in figure 5c, which is the projection of figure 5a on to the time axis. Thus, even if τ_c is not corrected for the overestimation, magnetars already occupy a considerable fraction of young NSs. If we replace τ_c of magnetars with their true ages, their dominance among young NSs will become even more enhanced.

As yet another important implication, we expect that numerous aged magnetar descendants would lurk in our

Galaxy. Radio pulsars, observed as the major population of NSs, cannot harbor such aged magnetars, because their P are shorter than those of magnetars. Instead, such objects may be being discovered as weak-field SGRs, including SGR 0418+5729 (Rea et al. 2013), Swift J1822.31606 (Rea et al. 2012; Scholz et al. 2012) and 3XMM J185246.6+003317 (Zhou et al. 2014).

8 Summary

We performed four pointings observations of CTB 109 with Suzaku. The spectra extracted from eastern parts of the SNR were well fitted with two plasma components that had two different temperatures. Assuming thermal equilibrium between electrons and protons, the shock velocity was calculated as 460 km s^{-1}, and the age of the SNR was estimated as 14 kyr using the Sedov-similarity solution. These results are consistent with the conclusion of the previous work by Sasaki et al. (2013). We thus reconfirmed the huge discrepancy between the age of CTB 109 and the characteristic age of 1E 2259+586.

We consider that the characteristic age of 1E 2259+586 is significantly overestimated, as compared to its true age which we identify with that of CTB 109. This effect, seen also in some other magnetars to a lesser extent, can be attributed to decay of their magnetic fields, as implied by the basic concept of "magnetars." In fact, the observed pulse period and its derivative of 1E 2259+586 has been explained successfully by a family of solutions to a simple equation describing the magnetic field decay. Furthermore, the τ_c versus τ_{SNR} relation of the three magnetar-SNR associations, including the 1E 2259+586/CTB 109 pair, can be explained consistently if they have a common value of α in the range of 0.6–1.4.

As a result, magnetars are considered to be much younger than was considered so far, and are rather dominant among new-born NSs. The youth of magnetars is supported independently by their much stronger concentration along the Galactic plane than ordinary pulsars.

Acknowledgments

This work was supported by JSPS KAKENHI Grant Number 12J09081.

References

Allen, M. P., & Horvath, J. E. 2004, ApJ, 616, 346
Baykal, A., Swank, J. H., Strohmayer, T., & Stark, M. J. 1998, A&A, 336, 173
Castro, D., Slane, P., Ellison, D. C., & Patnaude, D. J. 2012, ApJ, 756, 88
Chevalier, R. A. 2005, ApJ, 619, 839
Chevalier, R. A. 2011, AIP Conf. Proc., 1379, 5
Coe, M. J., & Jones, L. R. 1992, MNRAS, 259, 191
Coe, M. J., Jones, L. R., & Lehto, H. 1994, MNRAS, 270, 178
Colpi, M., Geppert, U., & Page, D. 2000, ApJ, 529, L29
Dall'Osso, S., Granot, J., & Piran, T. 2012, MNRAS, 422, 2878
Davies, S. R., Coe, M. J., Payne, B. J., & Hanson, C. G. 1989, MNRAS, 237, 973
Duncan, R. C., & Thompson, C. 1992, ApJ, 392, L9
Duncan, R. C., & Thompson, C. 1996, AIP Conf. Proc., 366, 111
Enoto, T., Nakazawa, K., Makishima, K., Rea, N., Hurley, K., & Shibata, S. 2010, ApJ, 722, L162
Esposito, P., et al. 2010, Astronomer's Telegram, 2691
Fahlman, G. G., & Gregory, P. C. 1983, in IAU Symp. 101, Supernova Remnants and their X-ray Emission, ed. J. Danziger & P. Gorenstein (Dordrecht: D. Reidel Publishing Co.), 445
Fahlman, G. G., Gregory, P. C., Middleditch, J., Hickson, P., & Richer, H. B. 1982, ApJ, 261, L1
Ferrand, G., & Safi-Harb, S. 2012, Adv. Space Res., 49, 1313
Gaensler, B. M. 2004, Adv. Space Res., 33, 645
Gavriil, F. P., & Kaspi, V. M. 2002, ApJ, 567, 1067
Gavriil, F. P., Kaspi, V. M., & Woods, P. M. 2004, AIP Conf. Proc., 714, 302
Ghavamian, P., Laming, J. M., & Rakowski, C. E. 2007, ApJ, 654, L69
Gregory, P. C., & Fahlman, G. G. 1980, Nature, 287, 805
Göğüş, E., Woods, P. M., Kouveliotou, C., Kaneko, Y., Gaensler, B. M., & Chatterjee, S. 2010, ApJ, 722, 899
Hanson, C. G., Dennerl, K., Coe, M. J., & Davis, S. R. 1988, A&A, 195, 114
Heydari-Malayeri, M., Kahane, C., & Lucas, R. 1981, Nature, 293, 549
Heyl, J. S., & Hernquist, L. 1999, MNRAS, 304, L37
Hobbs, G., Lorimer, D. R., Lyne, A. G., & Kramer, M. 2005, MNRAS, 360, 974
Hughes, V. A., Harten, R. H., & van den Bergh, S. 1981, ApJ, 246, L127
Hulleman, F., van Kerkwijk, M. H., Verbunt, F. W. M., & Kulkarni, S. R. 2000, A&A, 358, 605
Igoshev, A. P. 2012, ASP Conf. Proc., 466, 207
Ishisaki, Y., et al. 2007, PASJ, 59, S113
Iwasawa, K., Koyama, K., & Halpern, J. P. 1992, PASJ, 44, 9
Kaspi, V. M., Chakrabarty, D., & Steinberger, J. 1999, ApJ, 525, L33
Kaspi, V. M., Gavriil, F. P., & Woods, P. M. 2002, Astronomer's Telegram, 99
Kothes, R., & Foster, T. 2012, ApJ, 746, L4
Kothes, R., Uyaniker, B., & Yar, A. 2002, ApJ, 576, 169
Koyama, K., et al. 1989, PASJ, 41, 461
Koyama, K., et al. 2007, PASJ, 59, S23
Koyama, K., Hoshi, R., & Nagase, F. 1987, PASJ, 39, 801
Kumar, H. S., Safi-Harb, S., Slane, P. O., & Gotthelf, E. V. 2014, in IAU Symp. 296, Supernova Environmental Impacts, ed. A. Ray & R. A. McCray (Cambridge: Cambridge University Press), 235
Leahy, D. A., & Roger, R. S. 1991, AJ, 101, 1033
Lyne, A. G., & Graham-Smith, F. 1998, Pulsar Astronomy, 2nd ed. (Cambridge: Cambridge University Press)
Lyne, A. G., Pritchard, R. S., & Graham-Smith, F. 1993, MNRAS, 265, 1003

Lyons, N., O'Brien, P. T., Zhang, B., Willingale, R., Troja, E., & Starling, R. L. C. 2010, MNRAS, 402, 705
Manchester, R. N., Hobbs, G. B., Teoh, A., & Hobbs, M. 2005, AJ, 129, 1993
McKee, C. F., & Ostriker, J. P. 1977, ApJ, 218, 148
Mereghetti, S., Israel, G. L., & Stella, L. 1998, MNRAS, 296, 689
Nakagawa, Y. E., et al. 2009, PASJ, 61, S387
Nakamura, R., Bamba, A., Ishida, M., Nakajima, H., Yamazaki, R., Terada, Y., Phlhofer, G., & Wagner, S. J. 2009, PASJ, 61, 197
Pandey, U. S. 1996, A&A, 316, 111
Rea, N., et al. 2010, Science, 330, 944
Rea, N., et al. 2012, ApJ, 754, 27
Rea, N., et al. 2013, ApJ, 770, 65
Safi-Harb, S., & Kumar, H. S. 2013, IAU Symp. 291, Neutron Stars and Pulsars: Challenges and Opportunities after 80 years, ed. J. van Leeuwen (Cambridge: Cambridge University Press), 480
Sasaki, M., Kothes, R., Plucinsky, P. P., Gaetz, T. J., & Brunt, C. M. 2006, ApJ, 642, L149
Sasaki, M., Plucinsky, P. P., Gaetz, T. J., & Bocchino, F. 2013, A&A, 552, A45
Sasaki, M., Plucinsky, P. P., Gaetz, T. J., Smith, R. K., & Edgar, R. J. 2004, ApJ, 617, 322
Sato, T., Bamba, A., Nakamura, R., & Ishida, M. 2010, PASJ, 62, L33
Scholz, P., Ng, C.-Y., Livingstone, M. A., Kaspi, V. M., Cumming, A., & Archibald, R. F. 2012, ApJ, 761, 66
Sedov, L. I. 1959, Similarity and Dimensional Methods in Mechanics (New York: Academic Press)
Seward, F. D. 1985, Comment. Astrophys., 11, 15
Sofue, Y., Takahara, F., & Hirabayashi, H. 1983, PASJ, 35, 447
Staelin, D. H., & Reifenstein, E. C., III 1968, Science, 162, 1481
Tatematsu, K., Fukui, Y., Nakano, M., Kogure, T., Ogawa, H., & Kawabata, K. 1987, A&A, 184, 279
Tatematsu, K., Nakano, M., Yoshida, S., Wiramihardja, S. D., & Kogure, T. 1985, PASJ, 37, 345
Taylor, G. 1950, R. Soc. London Proc. Ser. A, 201, 159
Tendulkar, S. P., Cameron, P. B., & Kulkarni, S. R. 2012, ApJ, 761, 76
Tendulkar, S. P., Cameron, P. B., & Kulkarni, S. R. 2013, ApJ, 772, 31
Thompson, C., & Duncan, R. C. 1995, MNRAS, 275, 255
Torii, K., Tsunemi, H., Dotani, T., Mitsuda, K., Kawai, N., Kinugasa, K., Saito, Y., & Shibata, S. 1999, ApJ, 523, L69
Usov, V. V. 1992, Nature, 357, 472
Usov, V. V. 1994, ApJ, 427, 984
Vink, J. 2008, Adv. Space Res., 41, 503
Vink, J., & Kuiper, L. 2006, MNRAS, 370, L14
Woods, P. M., et al. 2004, AIP Conf. Proc., 714, 298
Zhou, P., Chen, Y., Li, X.-D., Safi-Harb, S., Mendez, M., Terada, Y. W., & Ge, M.-Y. 2014, ApJ, 781, L16